AIF and TUNEL staining

TUNEL staining was performed using an ApopTag Fluorescein In Situ Apoptosis Detection Kit (Merck Millipore) according to the manufacturer's instructions. Then, sections were incubated with rabbit anti-AIF antibody (1:100, AF1457, R&D Systems, Minneapolis, MN) at 4°C overnight. After being washed with PBS, the sections were incubated with Alexa Fluor 647-conjugated secondary antibody (Life Technologies) for 1 hr at RT, and the nuclei were counterstained with DAPI.

Cell viability assay of microglial cells

Microglial cells were plated on a 96-well poly-D-lysine (PDL)-coated plate at a density of 1.5×10^4 cells/well in Dulbecco's Modified Eagle Medium (DMEM, high glucose) containing fetal bovine serum (FBS) and incubated for 24 hr. After incubation, the medium was changed to DMEM containing FBS with (250 μM) or without (0 μM) menadione, and the cells were incubated for 24 hr. The cell viability was then measured using a Cell Counting Kit-8 (Dojindo, Kumamoto, Japan). The optical density of each well was measured by using a microplate reader at 490 nm.

Supplementary Figure 1

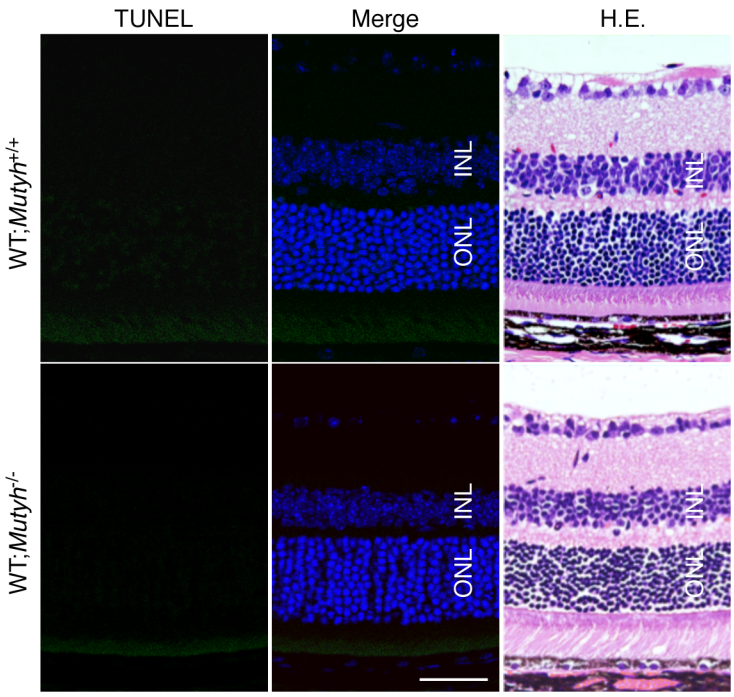

Supplementary Fig. S1. TUNEL staining and histological findings in the retinas of WT;*Mutyh*$^{+/+}$ and WT;*Mutyh*$^{-/-}$ mice. There were no histological differences between the WT;*Mutyh*$^{+/+}$ and WT;*Mutyh*$^{-/-}$ mice. HE, hematoxylin and eosin; INL, inner nuclear layer; ONL, outer nuclear layer. Scale bar: 50 μm.

Supplementary Figure 2

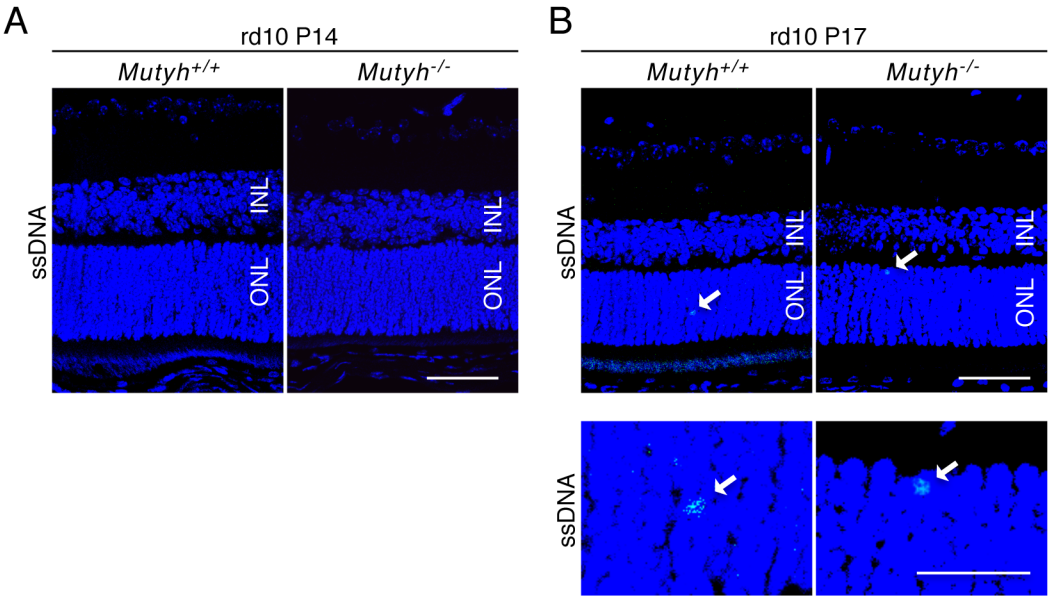

Supplementary Fig. S2. (A,B) SsDNA (green) and DAPI (blue) staining of ssDNA-positive cell in the retinas of P14 rd10;*Mutyh*$^{+/+}$ mice (A, left panel) and rd10;*Mutyh*$^{-/-}$ mice (A, right panel) and P17 rd10;*Mutyh*$^{+/+}$ mice (B, upper left panel) and rd10;*Mutyh*$^{-/-}$ mice (B, upper right panel). Higher magnification images of ssDNA-positive cell in the retinas of P17 rd10;*Mutyh*$^{+/+}$ mice (B, lower left panel) and rd10;*Mutyh*$^{-/-}$ mice (B, lower right panel). The arrowhead indicates co-localization of ssDNA and DAPI. There were no ssDNA-positive cells in the ONLs of the P14 rd10;*Mutyh*$^{+/+}$ mice or rd10;*Mutyh*$^{-/-}$ mice. Punctate staining of ssDNA were observed in the ONLs of the P17 rd10;*Mutyh*$^{+/+}$ mice and rd10;*Mutyh*$^{-/-}$ mice. INL, inner nuclear layer; ONL, outer nuclear layer. Scale bar: 50 μm (A and B, upper panels) and 20 μm (B, lower panels).

Supplementary Figure 3

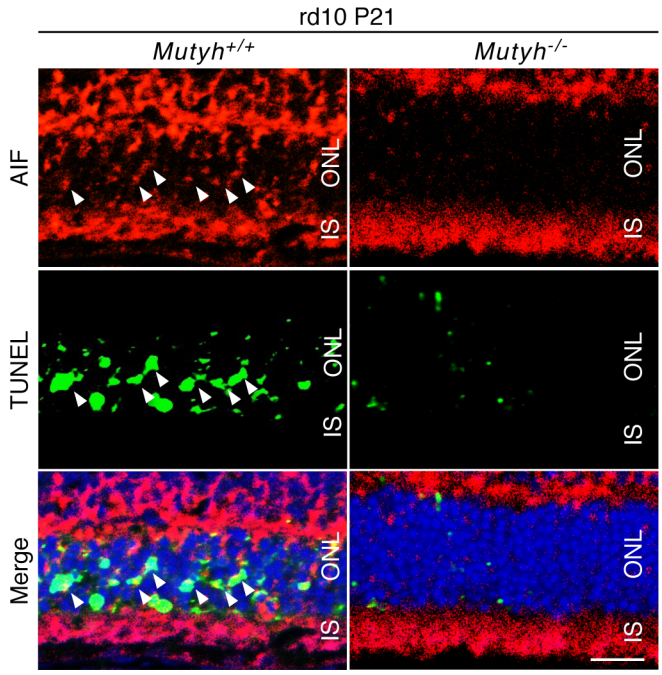

Supplementary Fig. S3. AIF (red) and TUNEL (green) staining in the retinas of P21 rd10;*Mutyh*$^{+/+}$ mice (left panel) and rd10;*Mutyh*$^{-/-}$ mice (right panel). The arrowheads indicate co-localization of AIF and TUNEL. IS, inner segment; ONL, outer nuclear layer. Scale bar: 20 μm.

Supplementary Figure 4

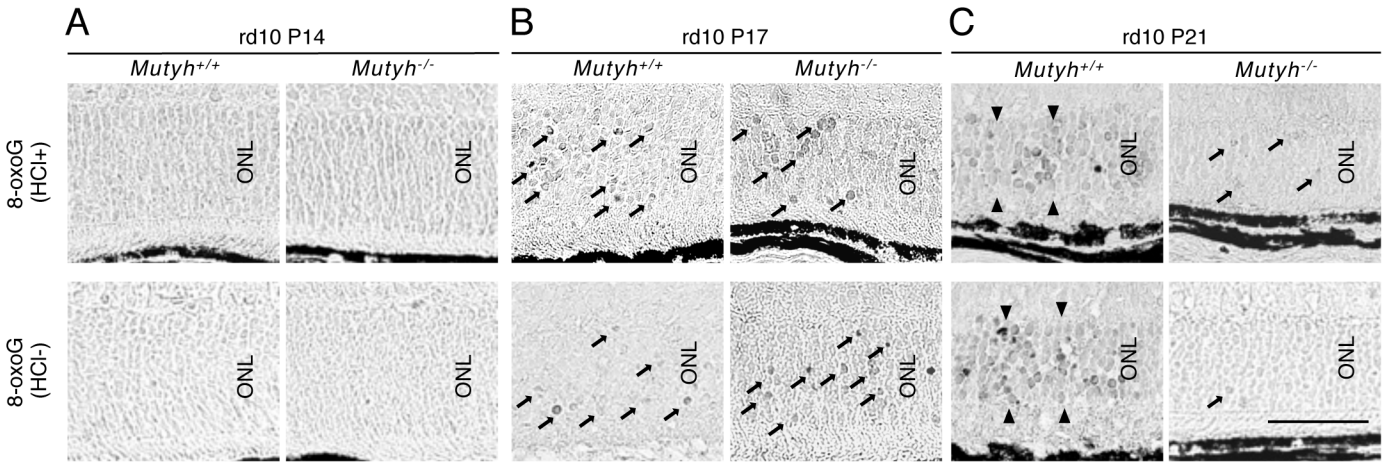

Supplementary Fig. S4. Higher magnification images of immunohistochemical detection of 8-oxoG in the retina of P14 (A), P17 (B) and P21 (C) rd10;*Mutyh*$^{+/+}$ mice and rd10;*Mutyh*$^{-/-}$ mice. These images are enlargements of the images shown in Figure 3. The accumulation of 8-oxoG was not observed in the retinas of rd10;*Mutyh*$^{+/+}$ mice and rd10;*Mutyh*$^{-/-}$ mice at P14 (A). Scattered accumulation of 8-oxoG was observed at P17 (arrows), and the staining pattern was comparable between the rd10;*Mutyh*$^{+/+}$ mice and the rd10;*Mutyh*$^{-/-}$ mice (B). The 8-oxoG accumulation was expanded to the ONL diffusely at the P21 rd10;*Mutyh*$^{+/+}$ mice (arrowheads), whereas it was substantially suppressed in the rd10;*Mutyh*$^{-/-}$ mice (arrows) (C). ONL, outer nuclear layer. Scale bar: 50 μm.

Supplementary Figure 5

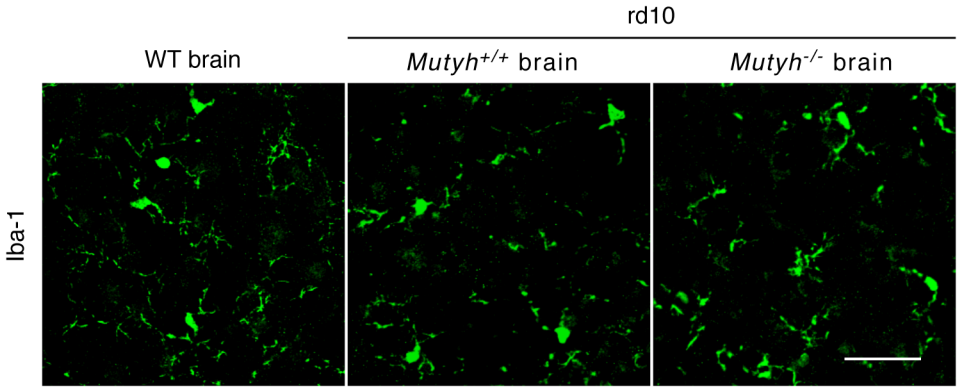

Supplementary Fig. S5. Immunostaining for Iba-1 in the brains of WT, rd10;*Mutyh*$^{+/+}$ and rd10;*Mutyh*$^{-/-}$ mice. There were no differences in the morphology of Iba-1-positive microglia between these mice. Scale bar: 50 μm.

Supplementary Figure 6

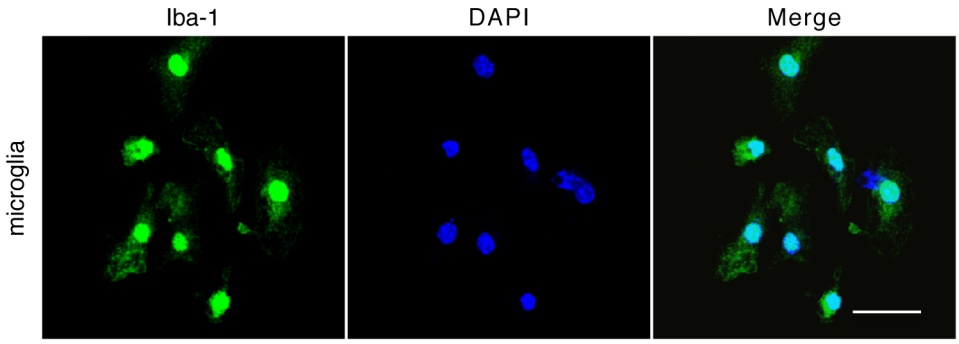

Supplementary Fig. S6. Immunocytostaining for Iba-1 in primary microglial cells. Iba-1 (green) and DAPI (blue) staining confirmed that >95% of the harvested cells were Iba-1-positive. Scale bar: 20 μm.

Supplementary Figure 7

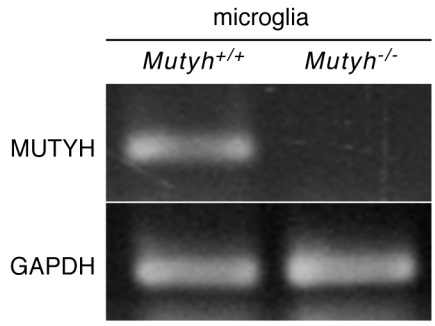

Supplementary Fig. S7. PCR for *Mutyh* in *Mutyh*$^{+/+}$ and *Mutyh*$^{-/-}$ microglia. MUTYH expression was abolished in the *Mutyh*$^{-/-}$ microglia.

Supplementary Figure 8

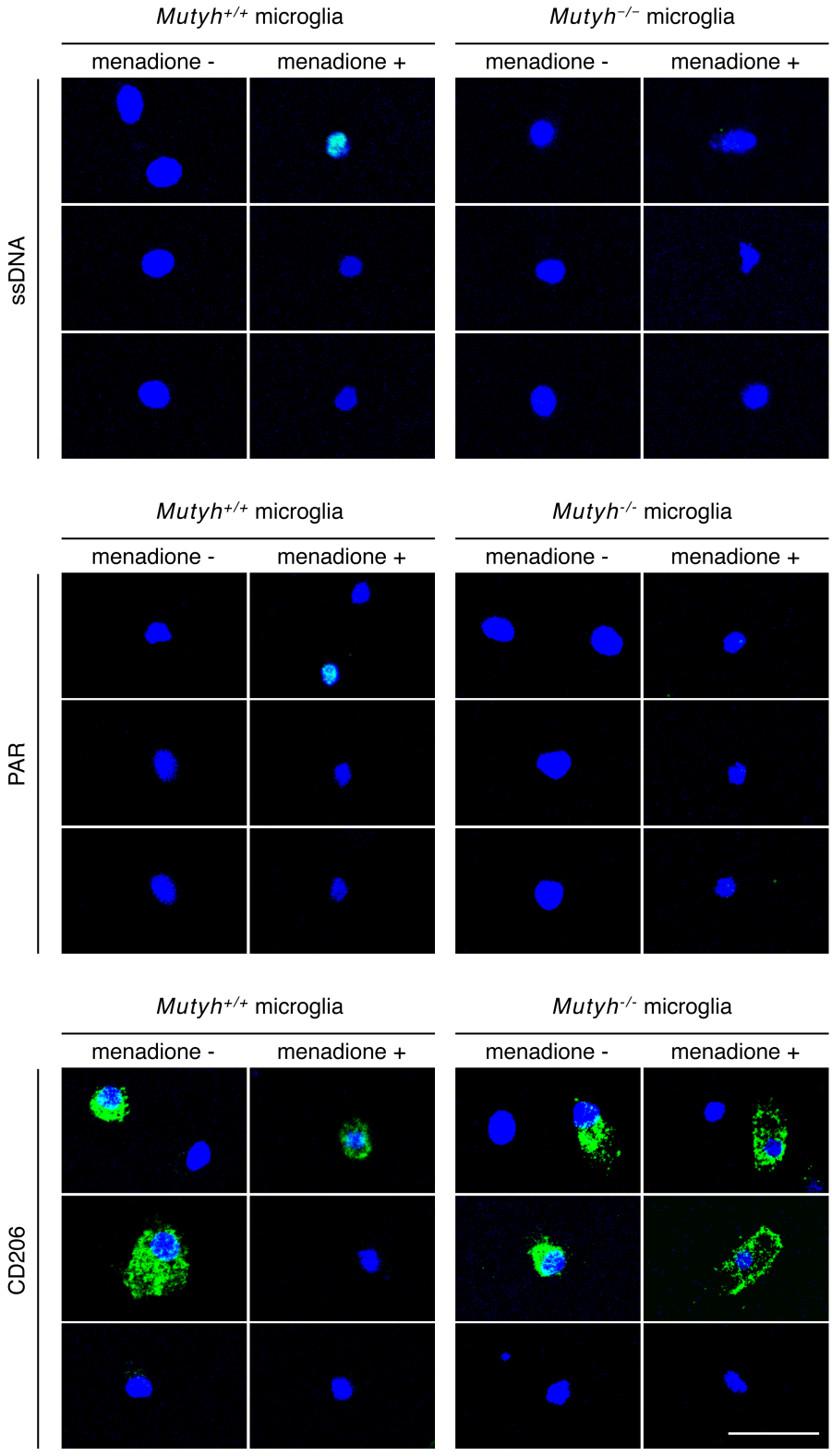

Supplementary Fig. S8. Representative immunostaining images of *Mutyh*$^{+/+}$ and *Mutyh*$^{-/-}$ microglia. ssDNA (green) and DAPI (blue) staining (upper row), PAR (green) and DAPI (blue) staining (middle row) and CD206 (green) and DAPI (blue) staining (lower row). Scale bar: 25 μm.

Supplementary Figure 9

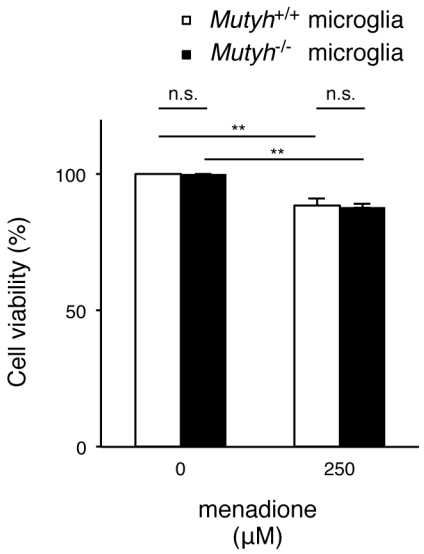

Supplementary Fig. S9. Cell viability assay of microglial cells. *Mutyh*$^{+/+}$ (n=10) or *Mutyh*$^{-/-}$ (n=11) microglia were treated in the presence or absence of 250 μM menadione for 24 hr. The cell viability of microglial cells was not severely affected by the menadione treatment, and there was no difference between the *Mutyh*$^{+/+}$ and *Mutyh*$^{-/-}$ microglia. Error bar: mean ± SEM. Data were analyzed by Student's t-test followed by Bonferroni correction. n.s., not significant.

**Bonferroni-corrected $p<0.01$.

Supplementary Figure 10

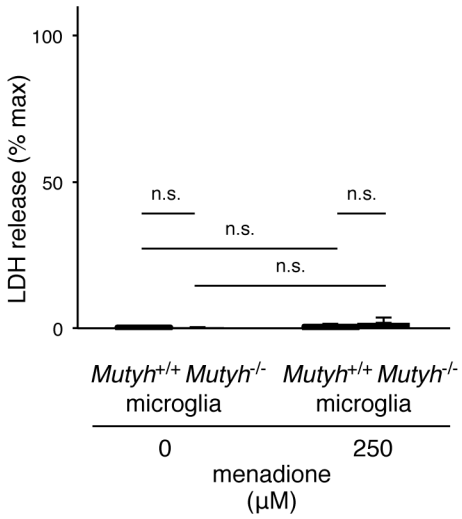

Supplementary Fig. S10. LDH release from microglial cells alone. *Mutyh*$^{+/+}$ (n=12) and *Mutyh*$^{-/-}$ (n=12) microglia were treated in the presence or absence of 250 μM menadione for 24 hr, and the supernatants were subjected to an LDH assay. The % cytotoxicity of each well was calculated as follows: (absorbance value of supernatant from each well / mean absorbance value of supernatants from 661W cells treated with Triton-X 100 well) × 100. Error bar: mean ± SEM. Data were analyzed by Student's t-test followed by Bonferroni correction. n.s., not significant.